Localization of CO_2 Gas Leakage through Acoustic Emission Multi-sensor Fusion Based on Wavelet-RBFN Modeling

Xiaojuan Han[1*], Song Zhao[1], Xiwang Cui[1,#], Yong Yan[2,1]

1. School of Control and Computer Engineering, North China Electric Power University, Beijing, China

2. School of Engineering and Digital Arts, University of Kent, Canterbury, UK

* Corresponding author. Tel.: 13001968881, E-mail address: hxj@ncepu.edu.cn

Abstract: CO_2 leakage from transmission pipelines in carbon capture and storage (CCS) systems may seriously endanger the ecological environment and human health. Therefore, an accurate and reliable leak localization method of CO_2 pipelines is a pressing need. In this study, a novel method based on the combination of wavelet packet algorithm and the radial basis function network (RBFN) is proposed to realize the leak localization. Multiple acoustic emission sensors are deployed to collect leakage signals of CO_2 pipelines firstly. The characteristics of the leakage signals from the AE sensors under different pressures are analyzed in both time and frequency domains. Further, leakage signals are decomposed into three layers using the wavelet decomposition theory. Wavelet packet energy and maximum value, time difference calculated by cross-correlation are selected as input feature vectors of the RBFN. Experiments were carried out on a laboratory-scale test rig to verify the validity and correctness of the proposed method. Leakage signals at different positions under different pressures were obtained on the CO_2 pipeline leakage test bench. Compared with the time difference of arrival (TDOA) method, the relative error obtained using the proposed method is less than 2%, which has certain engineering application prospects.

Keywords: Leak detection; Acoustic emission; Carbon capture and storage; Wavelet packet; Radial basis function network

1 Introduction

Carbon capture and storage technology is one of the most promising options to solve the global environmental crisis [1-2]. CO_2 transportation by the large-scale long-distance pipelines may pass through factories, ports and cities. Leakage accident will seriously endanger the ecological environment and human health [3]. Therefore, leak detection and localization of pipelines is indispensable for the CO_2 transportation.

At present, leak detection methods mainly include mass balance method, tracer method, imaging method, fiber optic method and acoustic emission (AE) method. Mass balance method [5] needs to be equipped with high accuracy mass flow sensors, but most of transmission pipelines are equipped with low accuracy flow meters for cost reasons. Tracer method [6] has a long operation time and a large workload, and it is difficult to realize on-line real-time detection of the pipeline. Image method includes thermal imaging method [7] and absorption imaging method [8]. It is difficult to continuously and real-time detect such long-scale equipment as pipelines using the image method [9]. In addition, the buried depth of the pipeline is also limited using the image method. The fiber optic method [10] has high precision of leak localization, however, it needs to

Currently with the Key Laboratory of Noise and Vibration Research, Institute of Acoustics, Chinese Academy of Sciences, Beijing, China

dig up the soil above the pipe for installation and maintenance. AE method [11-15] use a few of sensors to receive leakage signals propagating along the pipelines. It has the advantages of low cost, non-intrusiveness, fast response and high sensitivity. ***Yu et al***. [16] proposed a leak detection method on small leakage on galvanized steel pipelines based on AE technique, in which a support vector machine (SVM) method was used to detect the leaks. ***Mostafapour et al***. [17] proposed a leak localization algorithm based on wavelet transform and cross-correlation technique. Wavelet transform was used to remove the main noise of the leakage signals, and the leak localization was realized by the TDOA method. Results demonstrated that the localization error was less than 5%. ***Davoodi et al.*** [18] proposed a leak localization method using wavelet transform and cross-correlation. Through the signal decomposition and reconstruction, the localization error was reduced to less than 3%. ***Zhu et al.*** [19] used a model based on factor analysis and k-medoids clustering method for the leak localization and the error was less than 3.72%. ***Cui et al***. [20] proposed a weighted TDOA method based on the magnitude of the cross-correlation coefficient and empirical mode decomposition (EMD) algorithm with a localization error less than 5%. ***Yan et al***. [21] is proposed a near-field beamforming technique to locate the leak hole on the shell of a pressure vessel. The proposed method can scan the detection area with the localization error less than 4.1%. ***Tao et al***. [22] presented an improved multi-array TDOA localization algorithm to determine the precise leak location. A localization error less than 2 mm was achieved. ***Liao et al***. [23] proposed a method based on time delay estimation (TDE) which utilized three ultrasonic sensors arranged in an equilateral triangle. The leak can be located according to time delays between every two sensor signals.

In summary, the AE technology can effectively achieve the leak location, but the above-mentioned methods of detecting leak mainly focus on the cross-correlation method or the identification according to a certain leakage characteristic parameter, which has certain limitations.

Neural network is an effective method of the signal recognition relying on its good self-learning ability and strong adaptive ability [24]. ***Zadkarami et al***. [25] located the leak and determined its severity using the neural network. ***Alexandre et al***. [26] proposed a leak localization model using echo state neural networks and the results showed it was feasible.

Although neural network has the ability to reduce the noise effect and provide a quick analysis for a large number of data, the neural network structure and input characteristic parameters have a significant impact on the accuracy of leak location. Therefore, the main purpose of this study is to improve the localization accuracy through extracting the main characteristic parameters related to the pipeline leakage signals by wavelet packet decomposition. The time difference, wavelet energy and maximum value of the leakage signals obtained by the wavelet packet decomposition algorithm are regarded as the inputs of the RBFN and the leak position is regarded as the output of the RBFN. A pipeline leak localization model based on the combination of wavelet packet decomposition and RBFN is established under different pressure conditions.

2 Feature Extractions of Leakage Signal Based on Wavelet Packet Decomposition

2.1 Spectral analysis of leakage signals at different positions

The propagation path of leakage signal is related to various factors such as the location of the leakage source, the geometric structure of the detected object and the position where the acoustic signal sensors are distributed. In order to analyze the characteristics of the leakage signal at different locations, three pairs of sensors with an equal spacing of 2 m are placed on the CO_2 transmission pipeline as shown in **Fig.1**. Here, the location of the leakage source is defined as the

origin of the coordinates, then CH1=-180 cm, CH2=-160 cm, CH3=-140 cm, CH4=20 cm, CH5=40 cm and CH6=60 cm.

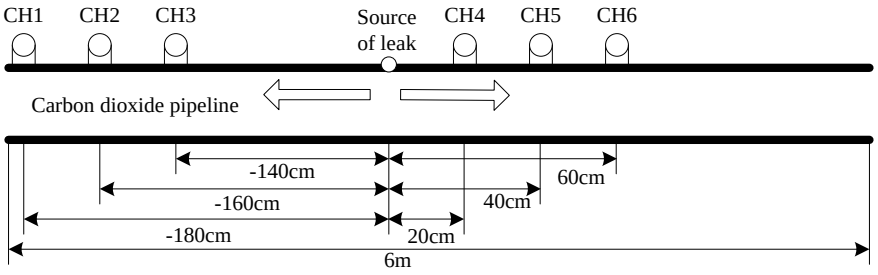

Fig.1 The installation position of the acoustic emission sensors

The frequency spectra of the leakage signals at different positions are shown in **Fig. 2**.

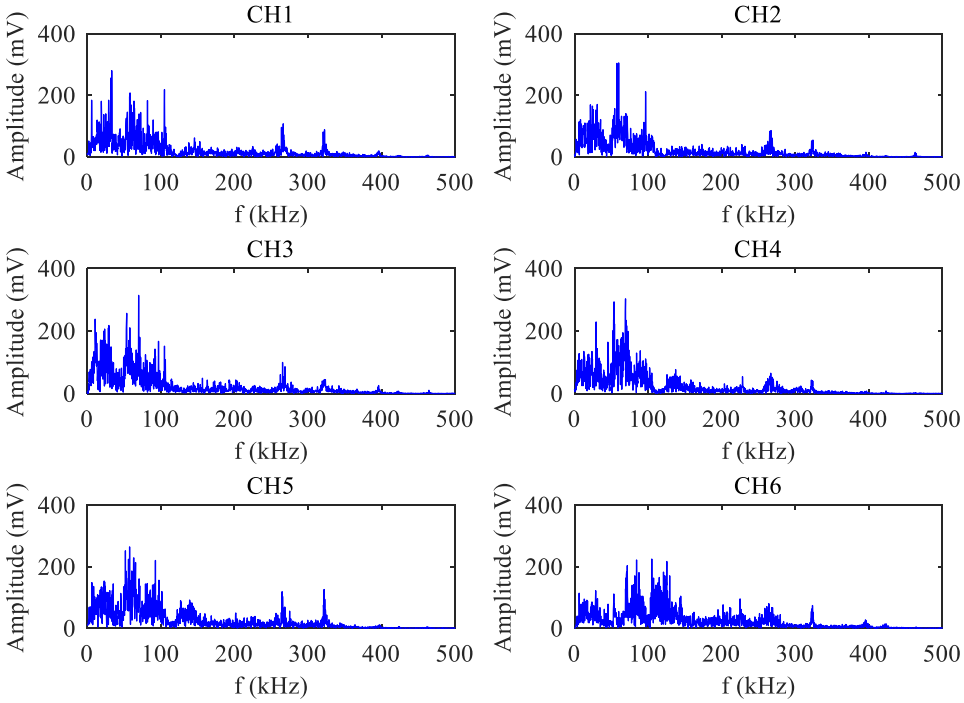

Fig.2 Frequency spectra of the leakage signals at different positions

It can be seen from **Fig.2** that the leakage signal is a non-stationary random signal containing many kinds of interference noise which randomly distributes over the entire sampling time range, so the time domain characteristics of the waveform cannot be detected separately. Similarly, it is not possible to detect the frequency domain characteristics of a wave signal in a single manner, so the two are combined to reflect the complete acoustic signal characteristics.

2.2 Amplitude extraction of leakage signals

With the increase of signal propagation distance, the energy attenuation, the corresponding signal amplitude attenuation trend will also be present. Signal amplitude can be selected as the feature vector of pipeline leak location. The extraction process of the signal amplitude characteristic is as follows:

Step1: The signals of the six channels are filtered by soft threshold to remove noise signals;

Step2: The signal of each channel is divided into three sections, and the maximum amplitude of each section is acquired;

Step3: The average value of the maximum amplitude for each section in the *i*th channel is regarded as the maximum amplitude value of the leak signal collected by the *i*th signal channel under different leak pressures, denoted as $X1_i^p$,(*i*=CH1, CH2…, CH6), p is the number corresponding to different leak pressures.

Eventually the maximum amplitude of each channel under different pressures is shown in **Table1**.

Table1 Maximum amplitude of each channel under different pressures

Pressure (MPa)	Amplitude (V)					
	CH1	CH2	CH3	CH4	CH5	CH6
0.1	0.0950	0.1289	0.1019	0.1160	0.1252	0.1028
0.2	0.2092	0.2456	0.2181	0.2644	0.2698	0.2374
0.3	0.4209	0.5313	0.3902	0.4763	0.4442	0.4256

2.3 Wavelet packet energy of leakage signals

Wavelet analysis can be used in multi-resolution analysis in the time and frequency domains because of its good sense of location [27-29]. Wavelet transform can represent the signal with low frequency information as the main component well, but it can't decompose and represent a lot of detailed information. In contrast to this, wavelet packet decomposition can divide the leak signals into multilevel frequency band and can be further decomposed high frequency part of leakage signal, which makes it more accurate in signal analysis as shown in **Fig.3**.

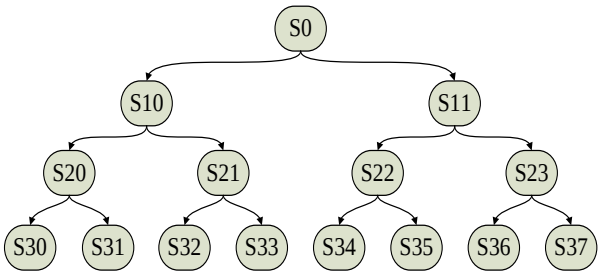

Fig.3 Schematic of three layer wavelet packet decomposition.

Wavelet packet decomposition algorithm is defined as follows:

$$\begin{aligned} d_{i,j,2n} &= \frac{1}{\sqrt{2}}\sum_k h_{0(k-2j)} d_{i+1,k,n} \\ d_{i,j,2n+1} &= \frac{1}{\sqrt{2}}\sum_k h_{1(k-2j)} d_{i+1,k,n} \end{aligned} \quad (1)$$

where $d_{i+1,k,n}$ is the upper wavelet packet decomposition results; $d_{i,j,2n}$ and $d_{i,j,2n+1}$ are the next level decomposition results of the wavelet packet decomposition; i is measure indicator; j is position indicator; n is the frequency index; k is the variable; h_0 and h_1 are multi-resolution filter coefficients[30].

Wavelet packet reconstruction algorithm is defined as follows:

$$d_{i+1,j,n} = \sum_k \left(h_{0(j-2k)} d_{i,k,2n} + h_{1(j-2k)} d_{i,k,2n+1} \right) \quad (2)$$

According to Parseval energy integral equation, the wavelet packet energy of the signals in time domain is defined as follows:

$$\left\|d_{i,j}\right\|^2 = \int_{-\infty}^{+\infty} \left|d_{i,j}\right|^2 dt \qquad (3)$$

The time domain waveform signals are shown in **Fig.4**.

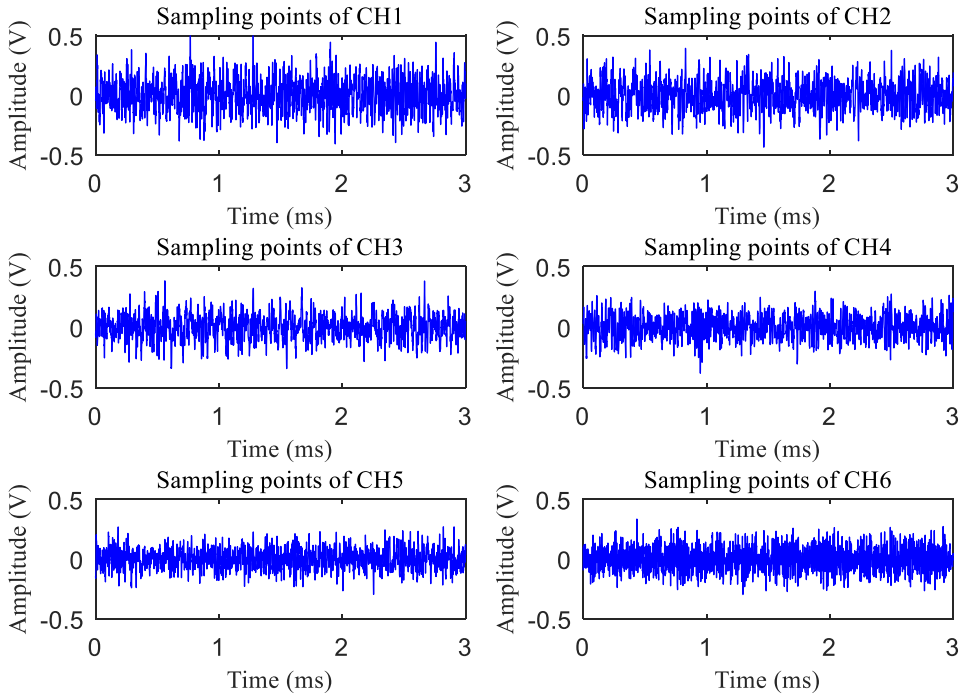

Fig.4 Time domain waveform signals under the pressure of 0.3MPa

Leakage signals are decomposed using wavelet packet algorithm and then wavelet packet decomposition coefficients.

The wavelet packet decomposition coefficients of the leak signals are decomposed by using wavelet packet when the leakage of pipelines located at the leakage point. The choice of mother wavelet has an important influence on the results of the analysis. In this study the signal is decomposed using db1 wavelet packet.

Extracting the third layer of signal and analysis respectively, the total signals can be represented as follows:

$$S0 = S30 + S31 + S32 + S33 + S34 + S35 + S36 + S37 \qquad (4)$$

Assume that the original signal *S*0, the lowest frequency component is 0, and the highest frequency component is 3MHz, the range of frequencies of eight components $S3_j(j = 0,1,\ldots,7)$ is shown in **Table 2**. The feature of the leakage signals extracted by wavelet packet from CH1 to CH6 (0.3Mpa) is shown in **Fig.5**.

Table 2 Frequency dimensions of every fact

Signal	*S*30	*S*31	*S*32	*S*33	*S*34	*S*35	*S*36	*S*37
Frequency （kHz）	0-375	375-750	750-1125	1125-1500	1500-1875	1875-2250	2250-2625	2625-3000

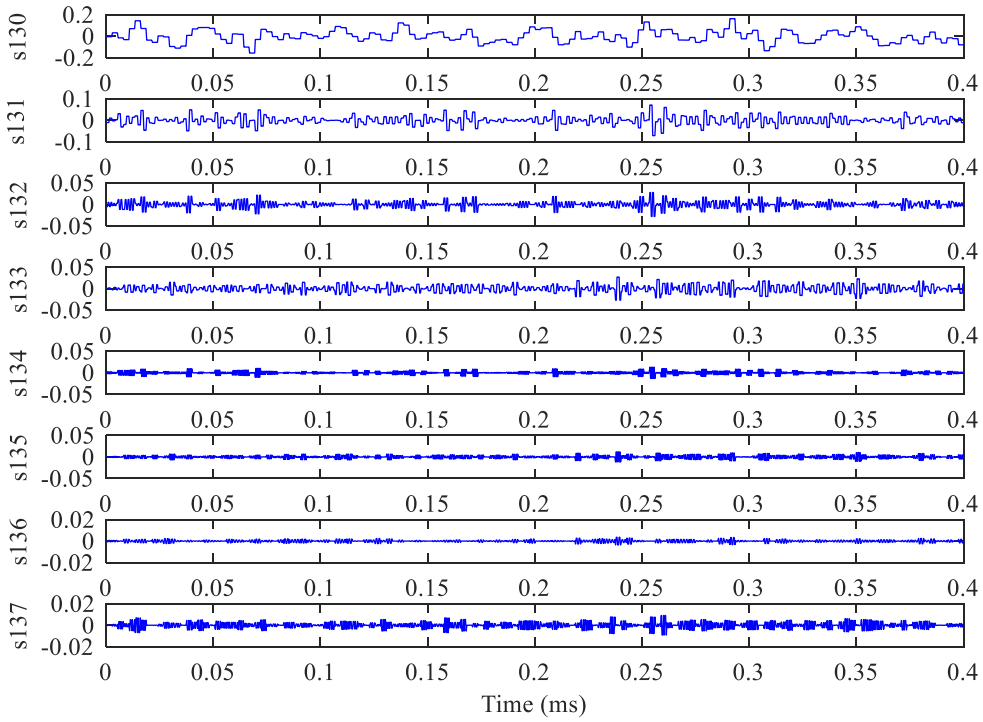
s130
s131
s132
s133
s134
s135
s136
s137
0.2
0
-0.2
0.1
-0.1
0.05
-0.05
0.02
-0.02
0
0.05
0.1
0.15
0.2
0.25
0.3
0.35
0.4
Time (ms)

(a)

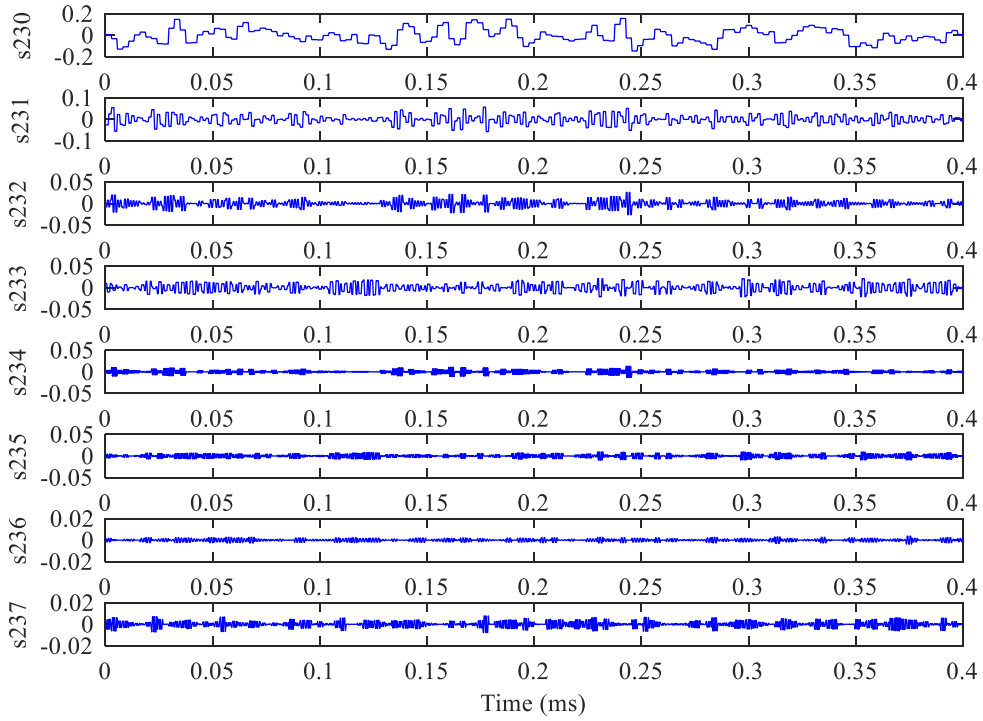
s230
s231
s232
s233
s234
s235
s236
s237
0.2
0
-0.2
0.1
-0.1
0.05
-0.05
0.02
-0.02
0
0.05
0.1
0.15
0.2
0.25
0.3
0.35
0.4
Time (ms)

(b)

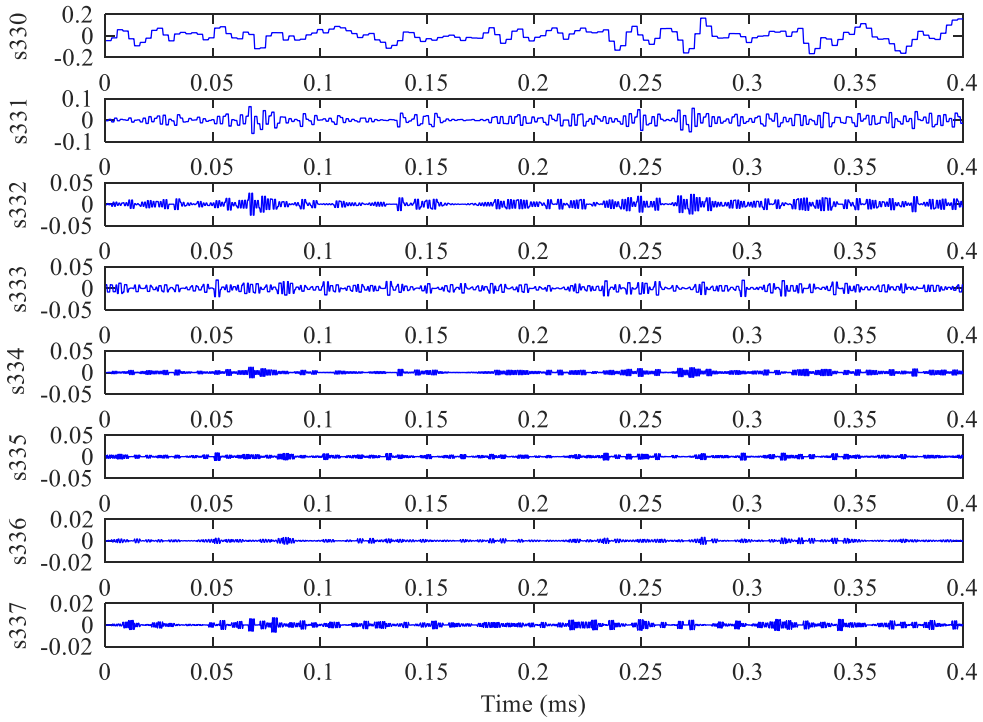
s330
s331
s332
s333
s334
s335
s336
s337
0.2
0
-0.2
0.1
-0.1
0.05
-0.05
0.02
-0.02
0
0.05
0.1
0.15
0.2
0.25
0.3
0.35
0.4
Time (ms)

(c)

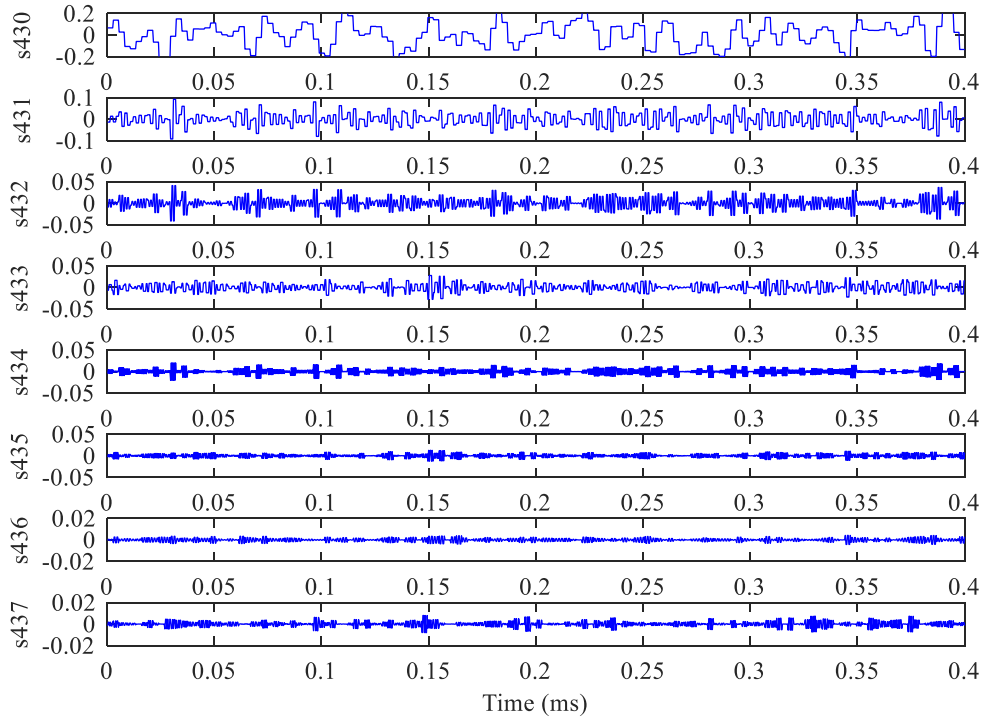
s430
s431
s432
s433
s434
s435
s436
s437
0.2
0
-0.2
0.1
-0.1
0.05
-0.05
0.02
-0.02
0
0.05
0.1
0.15
0.2
0.25
0.3
0.35
0.4
Time (ms)

(d)

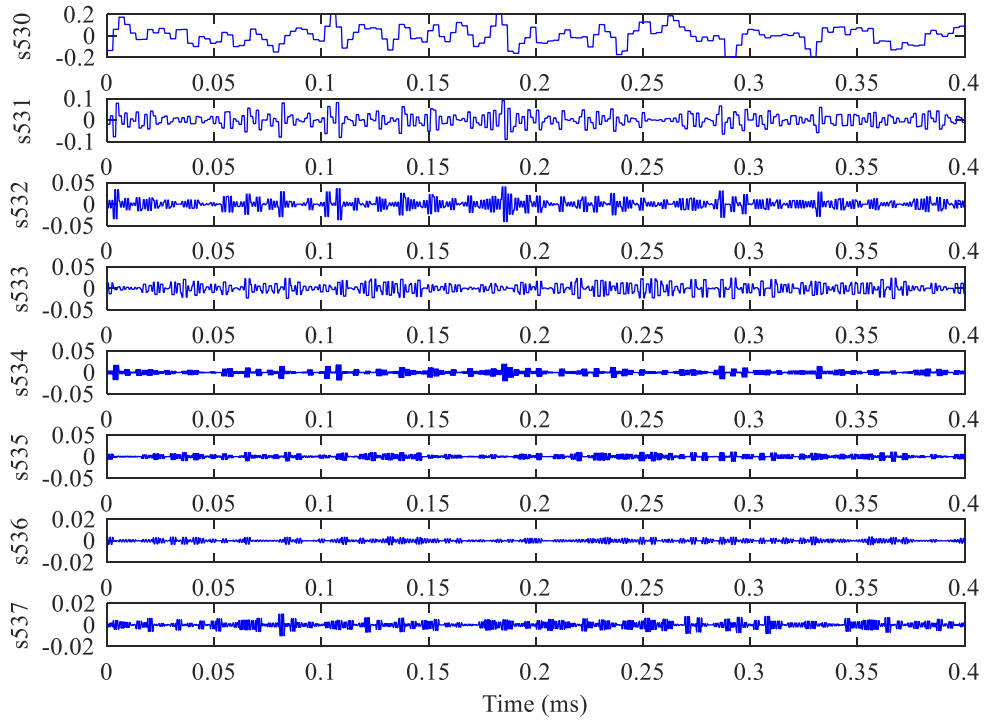

(e)

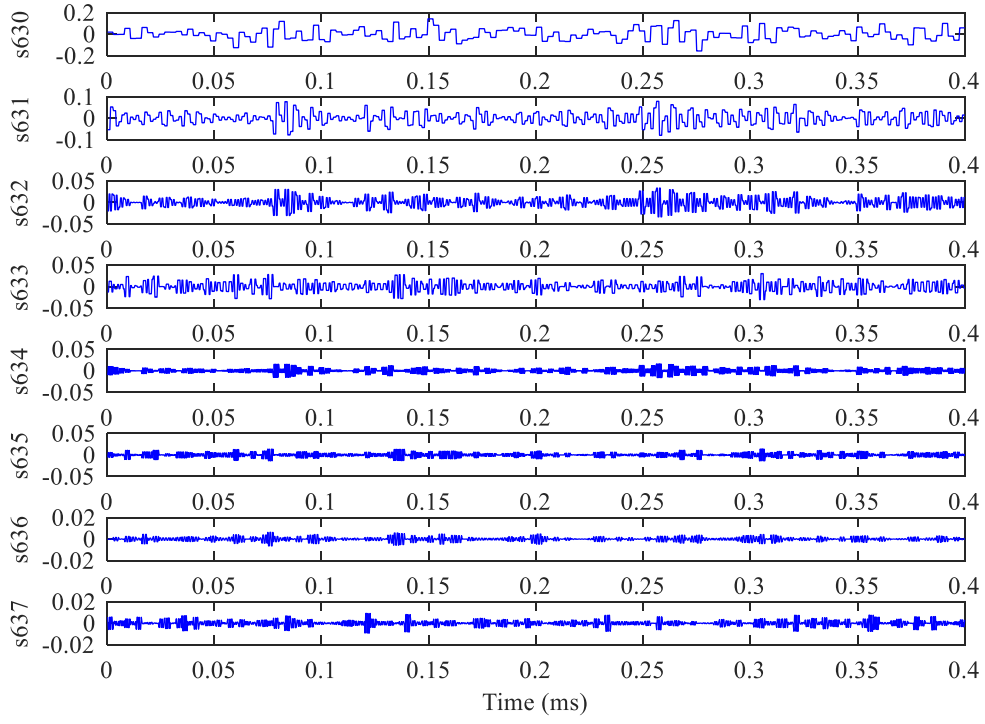

(f)

Fig.5 The features of the leakage signals extracted by wavelet packet from CH1 to CH6 (0.3Mpa)

Take an example to analyze the wavelet packet energy of each frequency band, it is shown in **Table 3.**

Table 3 The wavelet packet energy of each frequency band under the pressure of up to 0.3MPa

Pressure (MPa)	Channel	Amplitude							
		S30	S31	S32	S33	S34	S35	S36	S37

0.1	CH1	5.0334	2.7228	0.9423	1.6613	0.4451	0.7467	0.2305	0.5226
	CH2	4.6943	2.5524	0.9180	1.5180	0.4378	0.6841	0.2169	0.4831
	CH3	4.0737	2.8254	1.0676	1.3941	0.5156	0.6322	0.2050	0.4348
	CH4	3.0397	1.8056	0.6021	1.0871	0.2859	0.4883	0.1419	0.3506
	CH5	2.8284	2.1578	0.6425	1.4612	0.2978	0.6526	0.1715	0.4740
	CH6	3.4029	1.9471	0.6696	1.1655	0.3139	0.5255	0.1579	0.3651
0.2	CH1	5.8349	2.8972	1.1119	1.4867	0.5344	0.6772	0.2231	0.4533
	CH2	5.9070	2.7918	1.0556	1.4782	0.5060	0.6639	0.2216	0.4823
	CH3	5.5612	3.3310	1.3651	1.4554	0.6641	0.6697	0.2307	0.4185
	CH4	7.6100	3.4572	1.2980	1.8196	0.6252	0.8247	0.2583	0.5721
	CH5	6.3680	3.5702	1.3011	1.9862	0.6216	0.8993	0.2719	0.6031
	CH6	6.3229	2.9006	1.0960	1.5970	0.5245	0.7294	0.2392	0.4656
0.3	CH1	12.4840	4.2708	1.8270	1.7133	0.8942	0.7847	0.2679	0.5161
	CH2	12.7242	4.2465	1.8229	1.7375	0.8942	0.7917	0.2703	0.5215
	CH3	12.0996	5.8265	2.5511	2.1973	1.2459	1.0173	0.3654	0.6004
	CH4	14.7358	5.2662	2.1970	2.3822	1.0743	1.0850	0.3542	0.7177
	CH5	14.0106	5.5740	2.2040	2.8659	1.0723	1.2952	0.3798	0.9015
	CH6	13.8933	5.1440	2.0490	2.3096	0.9970	1.0472	0.3232	0.7269

It can be seen from **Table 3** that the measured signal mutation of the pipeline can be clearly obtained by the wavelet packet energy *S*30 which decays with distance. Therefore, the leak location is related to wavelet packet energy *S*30, denoted as $X2_i^p$.

2.6 Cross-correlation analysis of leak signals

In order to enhance the robustness of the leak localization system of the CO_2 pipeline, other type of feature vectors related to the leak should be selected. Here the time difference is chosen as one of the feature vectors. Because the [3,0] node of wavelet packet decomposition contains the characteristic frequency of the leakage signal, the cross-correlation analysis of the signal S30 of each channel of wavelet packet decomposition is taken to obtain the cross-correlation time difference of any two channels as a feature vector. The cross-correlation results for any two channels are shown in **Fig.6**.

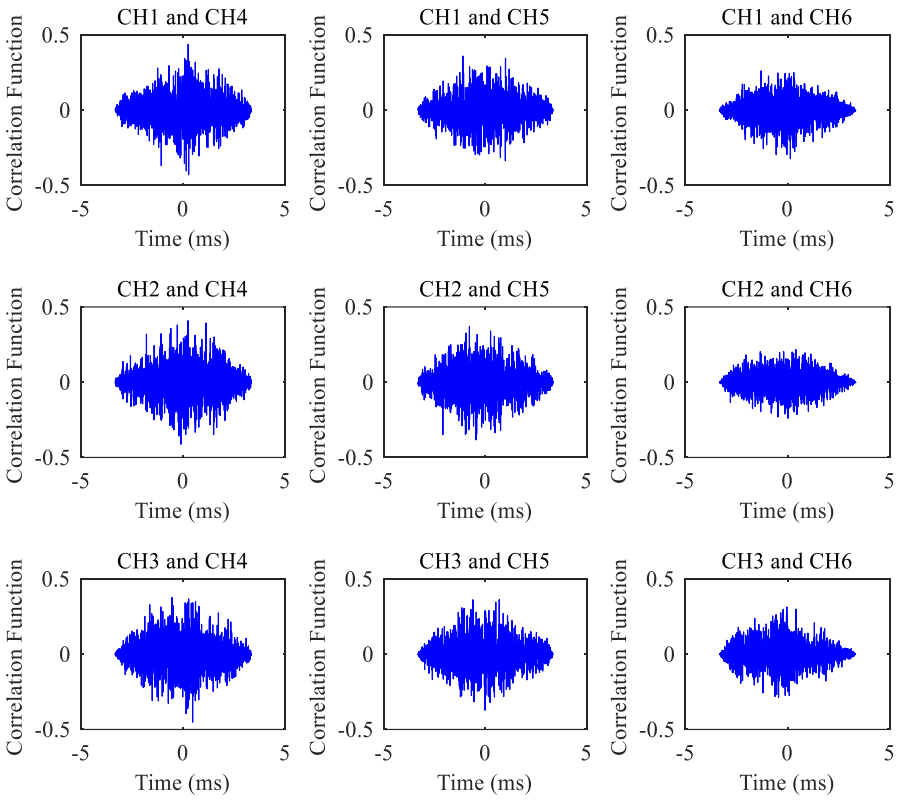

Fig.6 The cross-correlation results of any two channels (0.3Mpa)

It can be seen from Fig.6 that the peak of the cross-correlation function is not very clear and sharp. In some cases, there are several peaks with similar values. This phenomenon illustrates that leak localization method only based on the cross-correlation for time delay is not reliable. **Table 4** shows the results of time difference calculated by the cross–correlation function.

Table 4 Time difference between any two channels under different pressures

Pressure (MPa)	Time difference (ms)								
	CH1 CH6	CH1 CH5	CH1 CH4	CH2 CH6	CH2 CH5	CH2 CH4	CH3 CH6	CH3 CH5	CH3 CH4
0.1	0.2400	0.3013	**0.0960**	0.2520	0.2797	0.3427	0.0453	0.3360	0.3640
0.2	0.2577	0.2817	0.3033	0.1757	**0.1147**	0.2267	**0.3520**	0.2557	0.2530
0.3	0.1893	0.2507	**0.2160**	0.1760	0.1777	0.3227	**0.2090**	0.1387	0.1483

It can be seen from **Fig.6** and **Table 4** that when CH1, CH2 and CH3 are fixed, as the distances of CH4, CH5 and CH6 increase, the correlation coefficient decreases and the time difference between any two channels also decreases. Therefore, the time difference between two sensors based on the correlation coefficient is related to the leak location, which can be regarded as a feature vector to improve the accuracy of the leak location, denoted as $X3_{l,r}^{p}(l = 1,2,3; r = 4,5,6)$, where l is the channel number on the left of the leak source and r is the channel number on the right of the leak source. However, the time difference between the two sensors on the individual channels is abnormal, such as CH1-CH4 in the pressure of 0.1Mpa, CH2-CH5 and CH3-CH6 in the pressure of 0.2Mpa, CH1-CH4 and CH3-CH6 in the pressure of 0.3Mpa. This is because the AE sensors are influenced by unknown disturbance during collecting the leakage signal. Thus, leak localization using the time difference method based on the correlation coefficient alone will produce a large error (as shown in **Table 6**).

3 Leak localization of CO_2 pipelines based on the Wavelet-RBFN

3.1 Leak localization modeling of CO_2 pipelines based on the Wavelet-RBFN

The RBFN is well known in the field of approximation of nonlinear function and pattern recognition. In particular, the RBFN has a fast convergence property because of a simple architecture and a similar feature to the fuzzy inference system [31]. The peak signal $X1_{l,r}^{p}$ on both sides of the leakage source, the wavelet energy extracted by wavelet $X2_{l,r}^{p}$ on both sides of the leakage source and the time difference $X3_{l,r}^{p}$ on both sides of the leakage source are taken as the input of the RBFN, where $X1_{l,r}^{p}$, $X2_{l,r}^{p}$, $X3_{l,r}^{p}$ are described by (5).

$$\begin{aligned} X1_{l,r}^{p} &= \left[\mathrm{X1}_{l}^{p}, \mathrm{X1}_{r}^{p}\right] \\ X2_{l,r}^{p} &= \left[\mathrm{X2}_{l}^{p}, \mathrm{X2}_{r}^{p}\right] \\ X3_{l,r}^{p} &= \left[X3_{l,r}^{p}\right] \end{aligned} \tag{5}$$

When the leak of the CO_2 pipeline occurs, the energy will be changed greatly. Therefore, it can be used as an element of the feature vector to determine the leak location of the pipeline. Total feature vector is given in (6).

$$T = [X1_{l}^{p}, X1_{r}^{p}, X2_{l}^{p}, X2_{r}^{p}, X3_{l,r}^{p}] \tag{6}$$

When the energy is large, the value of $X1_{l}^{p}, X1_{r}^{p}, X2_{l}^{p}, X2_{r}^{p}, X3_{l,r}^{p}$ are large and not conducive to analysis. Here, the feature vector T is normalized as T'.

$$T' = [X_1', X_2', X_3', X_4', X_5'] \tag{7}$$

where $X_1' = \frac{X1_{l}^{p}}{E}$; $X_2' = \frac{X1_{r}^{p}}{E}$; $X_3' = \frac{X2_{l}^{p}}{E}$;$X_4' = \frac{X2_{r}^{p}}{E}$; $X_5' = \frac{X3_{l,r}^{p}}{E}$.

E is calculated by (8).

$$E = \sqrt{(X1_{l}^{p})^2 + (X1_{r}^{p})^2 + (X2_{l}^{p})^2 + (X2_{r}^{p})^2 + (X3_{l,r}^{p})^2} \tag{8}$$

After the training of the RBFN, the mathematical model of leak detection is obtained, and the leak localization model using the known sensor leak signals based on the combination of wavelet and RBF neural network is established in **Fig.7**.

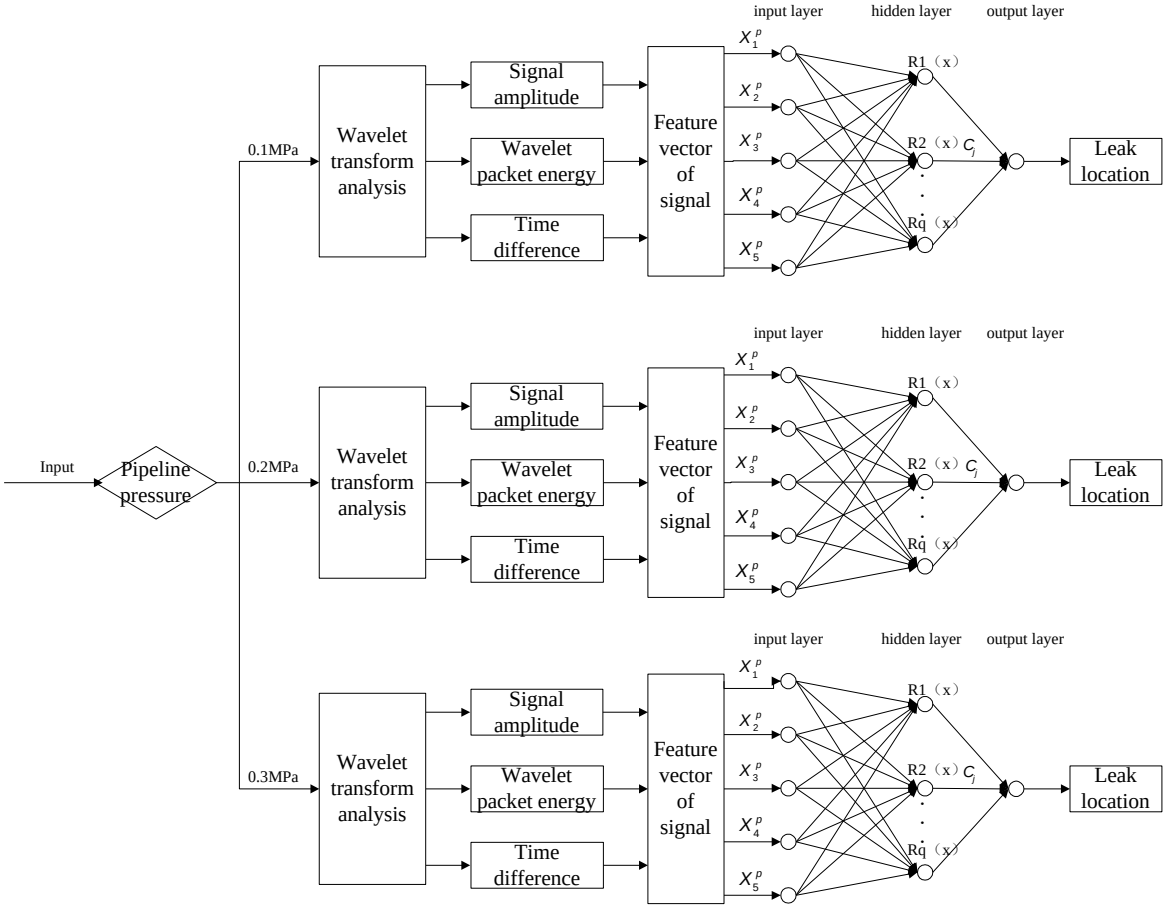

Fig.7 The architecture of a Wavelet-RBFN under different pressures

In this paper, the Gaussian function is selected as the receptive field unit and the weighted sum method is used to calculate the output of the RBFN, then the output is described as (9).

$$f = \sum_{j=1}^{q} c_j R_j(X)$$
$$R_j(X) = \exp\left(-\frac{\left\|X - m_j\right\|^2}{\delta_j^2}\right) \tag{9}$$

where q is the number of hidden nodes; c_j is the weight connecting the jth hidden node to the output node; $R_j(X)$ is the jth Gaussian function; $m_j \in R^N$ is the jth center vector; δ_j is the jth standard deviation. In this paper, the RBFN is used to realize the leak location of the CO_2 pipeline.

3.2 Leak localization process of the CO_2 pipeline based on the Wavelet-RBFN

The flow chart of the leak localization of the pipeline based on the Wavelet-RBFN is shown in **Fig.8**.

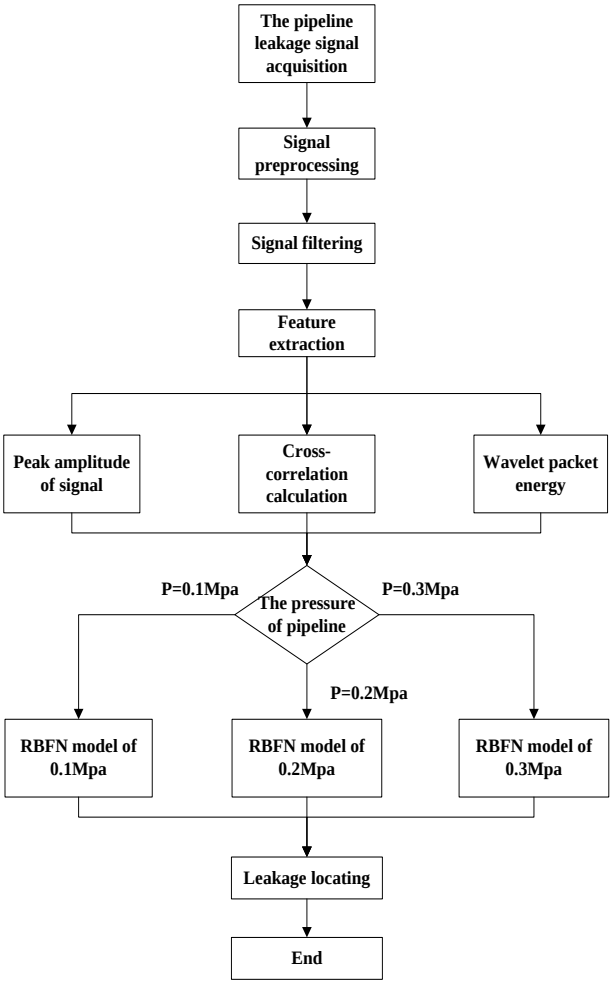

Fig.8 The flow chart of the leak location for the CO_2 pipeline

The specific steps of the leak location for the pipeline are as follows:

① Measure the temperature and pressure of the gas at the end of the simulated leak unit of the experimental device and judge the pressure of the pipeline. Here, the pressure of the pipeline is respectively chosen to be 0.1, 0.2 and 0.3 MPa.

② The leakage signals acquisition of the pipeline. Place six AE sensors with equal precision on the pipeline responding to Channel1～Channel6, the leak signal characteristics of the six signal channels under different leak pressures $\mathrm{X1}_{\mathrm{l,r}}^{\mathrm{p}}$, $\mathrm{X2}_{\mathrm{l,r}}^{\mathrm{p}}$, $\mathrm{X3}_{\mathrm{l,r}}^{\mathrm{p}}$ are extracted by adjusting the gas pressure in the pipeline.

③ Construct feature vector of the leak signals $T = [X1_l^p, X1_r^p, X2_l^p, X2_r^p, X3_{l,r}^p]$ and perform the normalization processing of the feature vectors on both sides of the leak source $T' = [X_1', X_2', X_3', X_4', X_5']$.

④ The feature vector T' under different leak pressures after normalization is used as the input of the RBFN, and the leak position value L is used as the output variable of the RBFN to establish the RBFN and training samples are adopted for the network training.

4 Case Analyses

4.1 Test bench construction of the CO_2 transport pipelines

The detection system based on acoustic emission sensors is composed of two parts: signal acquisition and signal processing. AE pipeline leak detection technology is actually the detection

of the acoustic signal frequency and voltage amplitude generated by the pipeline leak. In order to simulate the transmission pipeline, an experimental pipeline with the length of 6m and the outside diameter of 2inch at the laboratory is set up. A circular hole with 2 mm diameter is drilled in the position of 2 m from the left end of the pipeline. A schematic diagram of the experimental apparatus with liquid CO_2 stored in the tank of 5Mpa is shown in **Fig.9**. The valves are connected to the cylinders to regulate the outlet pressures of CO_2. When CO_2 is experiencing the leak hole in the pipeline, the acoustic signals will produce and propagate along the pipeline wall to the sides. In order to avoid echo phenomenon, the interface of the pipeline ends is set to the circular arc. Six sensors are placed on both sides of the leak source by the way of vacuum grease coupling agent with the equal interval of 2m, such as [CH1, CH4], [CH2, CH5], [CH3, CH6]. Taking the leak source as the coordinate center, sensors 1#, 2# and 3# are placed on the left side of the leak source, sensors 4#, 5# and 6# are placed on the right side of the leak source. The acoustic signals received by six sensors are converted into voltage signals at the range of [-1V, +1V]. Because these acoustic signals are very weak, the pre-amplifiers are installed at the rear side of each sensor to amplify the signals with the gain of 40dB. Finally, the leak signals collected by acquisition devices are fed into the computer.

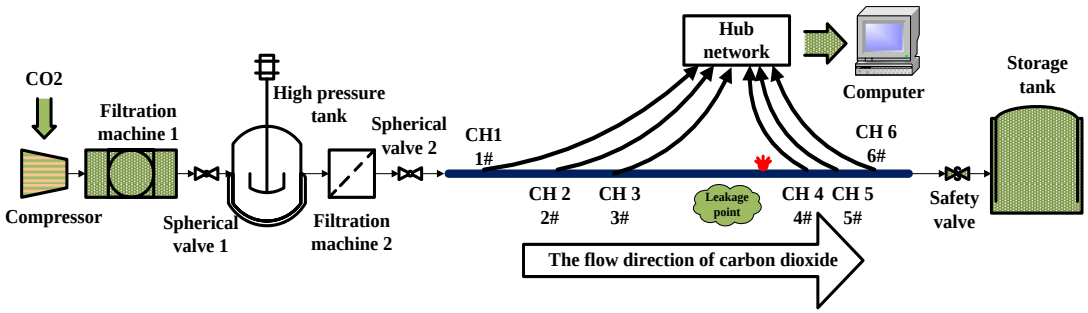

Fig.9 Schematic diagram of the laboratory experimental

4.2 Selection of acoustic emission sensor

In this paper, resonant high-sensitivity AE sensors are selected for leak signal acquisition. Resonant AE sensors have different sensitivity to signal response in different frequency bands and are often divided into low frequency sensors and high frequency sensors. According to the frequency range and amplitude range of the measured leak signal and noise signal, low frequency sensors are selected for the leak detection. The frequency response curves and physical parameters of low-frequency AE sensors used for the leak location of the CO_2 transport pipeline [15] are shown in **Fig.10** and **Table 5**.

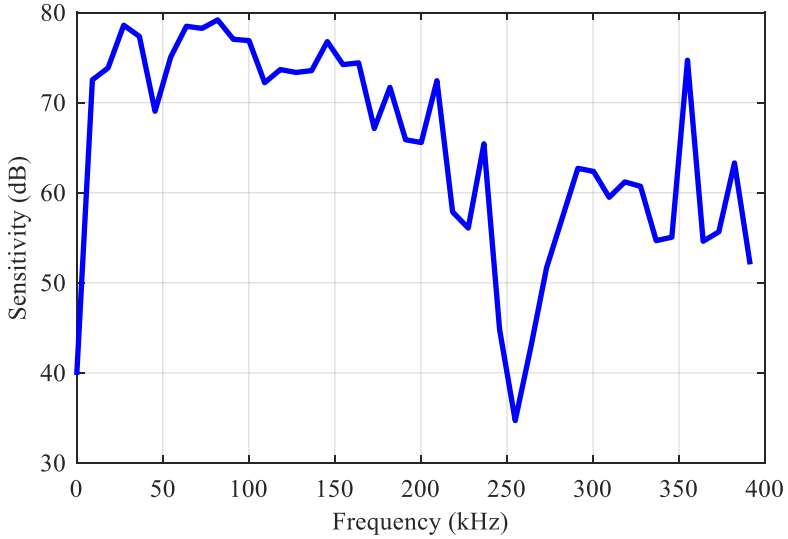

Fig.10 Frequency response of the AE sensor

Table 5 Technical specifications of the high frequency AE sensor

Size (Diameter*Height) (mm)	18.8*15
Operating temperature（ºC）	-20-200
Interface Type	M5-KY
Working frequency（kHz）	50-400
Peak sensitivity（dB）	>75

4.3 The actual leak location test device of the CO_2 pipeline

Due to the slender structure of the pressure pipeline, the diameter of the pipeline is almost negligible compared with the length of the pipeline, so the pipeline can be simplified to a one-dimensional linear model, and the sensors can be installed linearly on the pipeline. Through the analysis of the characteristics of the above CO_2 transport pipeline, it can be seen that the crack arrester and the pipeline block valve room are installed at intervals on the pipeline. Although the installation distance of these pipeline accessories has not yet been studied, it is generally on the order of several hundred meters to one kilometer. Low-frequency acoustic emission sensors are used to match high-power preamplifiers, and the detection distance can completely cover the installation spacing of these pipeline accessories. During the leak detection of the CO_2 transportation pipeline, the installation position of the sensors can be close to or coincided with the position of the crack arrester or the pipeline shut-off valve chamber, which not only facilitates the installation and overhaul of the sensors, but also reduces the construction difficulty and solves the waveform distortion of acoustic emission signals passing through these pipeline accessories. The actual leak location test device of the CO_2 pipeline corresponding to **Fig.9** is shown in **Fig.11**.

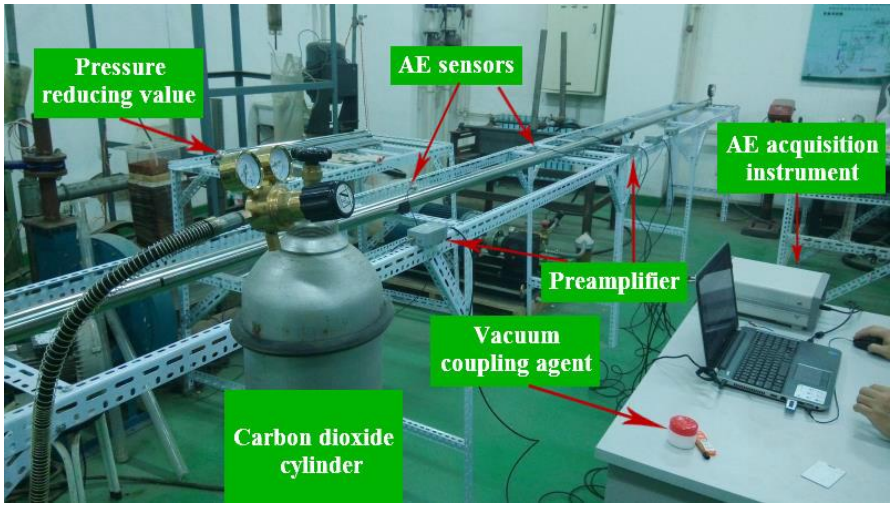

Fig.11 The actual leak test device of the CO_2 pipeline

4.4 The pre-process of the leak signals

The coupling conditions between the sensor and the pipeline are different in practice, so signals from different channels must be modified and fitted before extracting the characteristics. Taking the pipeline pressure as 0.3MPa as an example, the data collected by the six sensors from CH1 to CH6 is fitted by the least squares method. The data before and after the correction are shown in **Fig.12**.

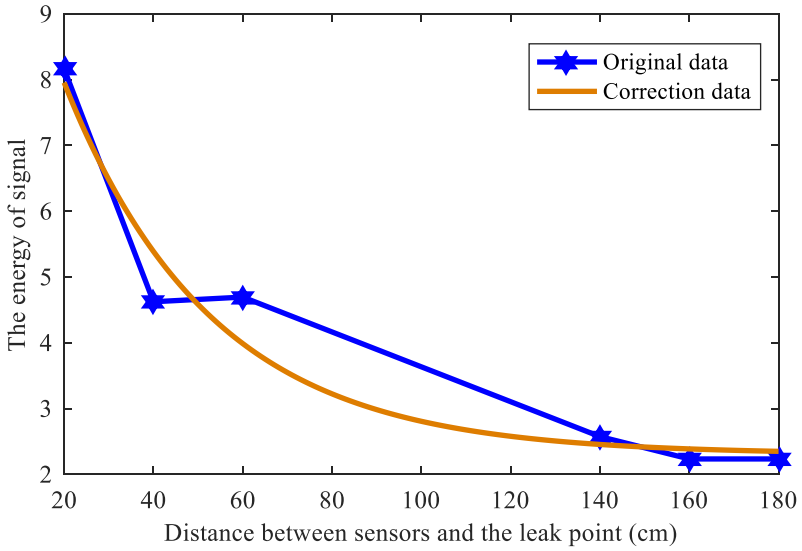

Fig.12 The data before and after the correction

It can be clearly seen from **Fig.12** that the energy of the signal received by the sensor gradually decreases as the distance between the sensor and the leak source increases.

4.5 Leak localization of the CO_2 pipeline method based on the TDOA

4.5.1 Localization principle based on the TDOA

Because the continuous AE signal generated by the leak source cannot be separated in the time domain, the traditional localization methods of AE sensors, such as the threshold method and the parameter method, are no longer suitable for the location calculation of the leak source. Therefore, the TDOA is used to achieve the leak localization of the CO_2 pipelines, which generally needs to install two or more sensors. The signals received by

the two sensors come from the same leak source, but there is a delay in the propagation time. Therefore, the position of the leak source can be calculated by the TDOA combining the propagation speed of the acoustic waves. Taking the signals from CH1=-180cm and CH4=20cm as an example, the localization principle based on the TDOA method is shown in **Fig.13**.

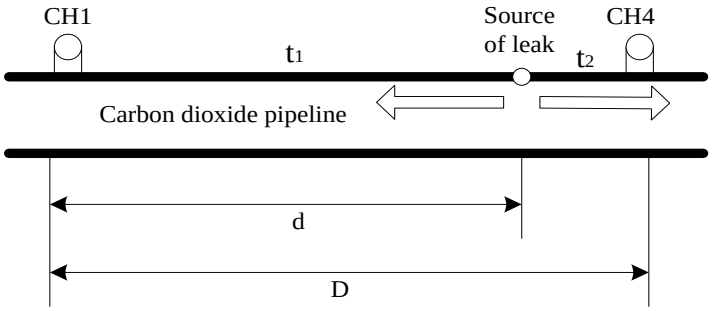

Fig.13 The localization principle based on the TDOA method

Assume that the required time for the signal generated by the leak source to propagate to CH1 and CH4 is t_1 and t_2 respectively, and the propagation velocity of acoustic waves at the wall of the pipeline is v, then the following relationship can be obtained by (10).

$$\begin{aligned} d &= vt_1 \\ D - d &= vt_2 \end{aligned} \tag{10}$$

where d is the distance from the leak source to CH1 and D is the distance between the two sensors. When the installation of the two sensors is complete, D is known (here D is equal to 2m), so only the value of d needs to be calculated to locate the leak source. The above equation can be simplified to (11).

$$d = \frac{D - v\Delta t}{2} \tag{11}$$

where Δt is the time difference between the two sensors receiving the signal.

It can be seen from (11) that the location of the leak source is related to only two parameters: one is the propagation speed of sound waves on the pipeline, and the other is the time difference of the signals received by the sensors.

4.5.2 Time difference extraction method based on wavelet packet decomposition

When the time difference of the signals between CH1=-180cm and CH4=20cm is measured, since the signals of the sensors at both ends have similarity, the equivalent signal segment is used to analyze the correlation coefficient segment by segment. The time difference corresponding to the maximum value of the cross-correlation function is defined as Δt, which is used to achieve the positioning of the leak source. Firstly, the collected signals are decomposed by wavelet packet, and the reconstructed signals of any two channels of S30 nodes are selected for the cross-correlation analysis. The noise signal and the leak signal are regarded as mutually independent irrelevant signals, then

$$R_{xy}(m) = \frac{\sum_{k=0}^{N-|m|-1} x_k y_{k+m}}{\sqrt{\sum_{k=0}^{N-1} x_k^2} \sqrt{\sum_{k=0}^{N-1} y_k^2}} \tag{12}$$

where x_k, y_k are the signals acquired by the two sensors; N is the signal length; R_{xy} is the cross-correlation function, meanwhile the time corresponding to the maximum correlation point of the cross-correlation function is the time difference between the signals received by the two

sensors.

In the absence of a leak, the signals collected by both sensors are noise and uncorrelated, so the value of cross-correlation function is approximately to zero; when a leak occurs, the corresponding peak value is at the most relevant moment, that is

$$R_{xy}(\tau_0) = \max[R_{xy}(\tau)] \tag{13}$$

The cross-correlation function between CH1 and CH4 under the pressure of 0.3MPa is shown in **Fig.14**. The sampling frequency is 3M, and 10000 points of the data are used to detect the leak location of the CO_2 pipelines, equaling to a time length of 1/300s.

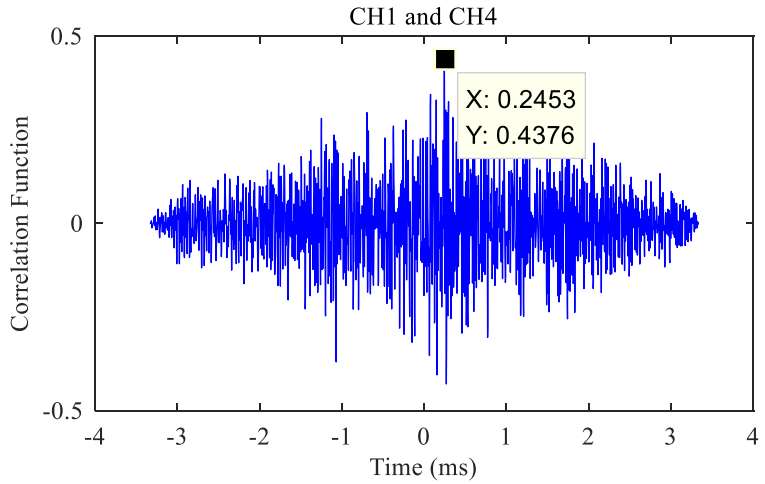

Fig.14 Cross-correlation curve between CH1 and CH4 under the pressure of 0.3MPa

The localization results of the sensors from CH1 to CH6 under different pressures are shown in **Fig.1** are given in **Table 6**.

Table 6 Localization results in different positions and different pressures

0.1Mpa				
Test sensors	Time difference（ms）	Leakage location（m）	Actual location（m）	Relative error（%）
CH1,CH6	0.24	1.8168	1.8	0.93
CH1,CH5	0.3013	1.9276	1.8	7.09
CH1,CH4	0.096	0.6867	1.8	61.85
CH2,CH6	0.252	1.8776	1.6	17.35
CH2,CH5	0.2797	1.8181	1.6	13.63
CH2,CH4	0.3427	1.9375	1.6	21.09
CH3,CH6	0.04533	0.8293	1.4	40.76
CH3,CH5	0.336	2.1035	1.4	50.25
CH3,CH4	0.364	2.0455	1.4	46.11
0.2Mpa				
Test sensors	Time difference（s）	Leakage location（m）	Actual location（m）	Relative error（%）
CH1,CH6	0.2577	1.9065	1.8	5.92
CH1,CH5	0.2817	1.6282	1.8	9.54
CH1,CH4	0.3033	1.7377	1.8	3.46
CH2,CH6	0.1757	1.4908	1.6	6.83
CH2,CH5	0.1147	0.9814	1.6	38.66
CH2,CH4	0.2267	1.3494	1.6	15.66
CH3,CH6	0.3520	1.9846	1.4	41.76
CH3,CH5	0.2557	1.6964	1.4	21.17
CH3,CH4	0.2530	1.4827	1.4	5.91
0.3Mpa				
Test sensors	Time difference（s）	Leakage location（m）	Actual location（m）	Relative error（%）
CH1,CH6	0.1893	1.5598	1.8	13.34
CH1,CH5	0.2507	1.8710	1.8	3.94
CH1,CH4	0.2160	1.6951	1.8	5.83

CH2,CH6	0.1760	1.2923	1.6	19.23
CH2,CH5	0.1777	1.3009	1.6	18.69
CH2,CH4	0.3227	2.0361	1.6	27.26
CH3,CH6	0.2090	1.2596	1.4	10.03
CH3,CH5	0.1387	1.1032	1.4	21.2
CH3,CH4	0.1483	1.3519	1.4	3.44

It can be seen from **Table 6** that the maximum errors reach 61.85% in the pressure of 0.1Mpa, 41.76% in the pressure of 0.2Mpa and 27.26% in the pressure of 0.3Mpa. Thus, only using the TDOA method for the leak localization cannot meet the engineering needs of the positioning accuracy. Therefore, in order to overcome the limitations of the algorithm and improve the localization accuracy, a localization method based on the combination of the wavelet and RBFN is proposed.

4.6 Leak localization of the CO_2 pipeline based on the Wavelet-RBFN

According to **Section 3**, the feature vectors composed of multiple wavelet eigenvalues on [-120, 80], [-100, 100], [-80,120] are regarded as the training samples of the RBFN, denoted as $T'_{train}$and the feature vectors composed of multiple wavelet eigenvalues on [-180,20], [-160,40], [-140,60] are respectively regarded as the testing samples of the RBFN, denoted as T'_{test}. The localization accuracy of the RBFN is related to the spread factor of the radial basis function. The larger the spread factor is, the smoother the function fit is. However, the approximation error becomes larger and the more hidden neurons lead amount of calculations increasing. The smaller the spread factor is, the more accurate the approximation of the function will be. However, the approximation process is not smooth, and the network performance is poor, and there will be an adaptation phenomenon. Therefore, different values of spread factor should be tried, and to the spread factor minimize the locating errors should be chosen. Under the three pressure conditions of 0.1Mpa, 0.2Mpa and 0.3Mpa, the leak localizations of the CO_2 pipelines located on [CH1,CH4],[CH2,CH5],[CH3,CH6] are performed, the results are shown in **Table 7**.

Table 7 Leak localization results under different pressures

0.1Mpa					
Test sensors	Real position （cm）	Leak location （cm）	Spread	Wavelet-RBFN	TDOA
				Relative error（%）	Relative error（%）
CH1-CH4	[-180,20]	[-178.5457,21.4543]	2.2	0.81	61.85
CH2-CH5	[-160,40]	[-162.1170,37.8830]	1.9	1.32	13.63
CH3-CH6	[-140,60]	[-139.8651,60.1349]	1.4	0.1	40.76
0.2Mpa					
Test sensors	Real position （cm）	Leak location （cm）	Spread	Wavelet-RBFN	TDOA
				Relative error（%）	Relative error（%）
CH1-CH4	[-180,20]	[-177.1581,22.8419]	1.9	1.58	3.46
CH2-CH5	[-160,40]	[-158.1776,41.8224]	1.7	1.14	38.66
CH3-CH6	[-140,60]	[-141.8791,58.1209]	1.5	1.34	41.76
0.3Mpa					
Test sensors	Real position （cm）	Leak location （cm）	Spread	Wavelet-RBFN	TDOA
				Relative error（%）	Relative error（%）
CH1-CH4	[-180,20]	[-180.1599,19.8401]	2.0	0.09	5.83
CH2-CH5	[-160,40]	[-161.5088,38.4912]	1.7	0.94	18.69
CH3-CH6	[-140,60]	[-141.5603,58.4379]	1.3	1.11	10.03

It can be seen from **Table 7**, the higher the pressure is, the stronger the signal strength is, and the higher the accuracy of the leak location will be. Under different pressures and positions, the minimum error of the leak location of the CO_2 pipelines using the Wavelet-RBFN reaches 0.09%, and the maximum error is only 1.58%. The minimum error of the leak locating of the CO_2 pipeline

using the TDOA method is 3.46%, and the maximum error is 61.85%. Therefore, the leak localization accuracy of the CO_2 pipeline based on the Wavelet-RBFN proposed in this paper is much higher than simply using the TDOA method. As the pressures of CO_2 gas in the pipeline increasing, the positioning error of the two methods tends to be decreased. The test results of experimental data show that the leak localization system based on the wavelet and RBFN has the characteristics of high accuracy and small errors, and has obvious superiority in the positioning approaches.

5 Conclusions

Through the analysis of the characteristics of CO_2 pipeline leakage signal, a localization method based on wavelet and RBFN has been proposed. Starting from the time-frequency characteristics of the pipeline leakage signal, according to the multi-sensor information fusion theory, the main signal characteristics reflecting the pipeline leakage are extracted, and the nonlinear learning characteristics of the neural network are used to realize the accurate localization of the CO_2 pipeline leakage. The main results are as follows:

1) Since the acoustic emission signal exists many kinds of interference noise in the real-life acoustic emission signal, the combination of the time domain and frequency domain characteristics of the leak signals based on multi-sensor fusion can improve the leak localization accuracy of the CO_2 pipeline to overcome the uncertainty of a single sensor.

2) For comparative analysis, the TDOA and Wavelet-RBFN methods are used to realize the leak localization of the CO_2 pipelines according to the leakage signals collected under different locations and different pressure conditions. The maximum error obtained only by the TDOA reaches 61.85%, and the maximum error obtained by the Wavelet-RBFN only is 1.58%. The above results verify the effectiveness of the proposed method.

Reference

[1] Aminu M D, Nabavi S A, Rochelle C A, *et al.* A review of developments in carbon dioxide storage[J]. Applied Energy, 2017,208:1389-1419.

[2] Fan J, Xu M, Li F, *et al.* Carbon capture and storage (CCS) retrofit potential of coal-fired power plants in China: The technology lock-in and cost optimization perspective [J]. Applied Energy, 2018, 229:326-334.

[3] Vianello C, Mocellin P, Macchietto S, *et al.* Risk assessment in a hypothetical network pipeline in UK transporting carbon dioxide[J]. Journal of Loss Prevention in the Process Industries, 2016,44:515-527.

[4] D'Amore F, Mocellin P, Vianello, *et al.* Economic optimisation of European supply chains for CO_2 capture, transport and sequestration, including societal risk analysis and risk mitigation measures [J]. Applied Energy, 2018, 223:401-415.

[5] Liu L, Yue Y, Huang J, *et al.* Think More about the Instruments Factors for the Mass Balance Type Pipeline Leak Detection Systems[C]. International conference on pipelines and trenchless technology, 2013,174-183.

[6] Ghazi C J, Marshall J S. A CO_2 tracer-gas method for local air leakage detection and characterization[J]. Flow Measurement and Instrumentation, 2014, 38:72-81.

[7] Sha M, Ghazali K H, Gas leakage detection using thermal imaging technique[C]. International Conference on Computer Modelling and Simulation, 2015,302-306.

[8] Zhao L, Yang H. Small-target leak detection for a closed vessel via infrared image sequences[J]. Infrared Physics & Technology, 2016, 81:109-116.

[9] Kasai N, Tsuchiya C, Fukuda T, *et al.* Propane gas leak detection by infrared absorption using carbon infrared emitter and infrared camera[J]. Ndt & E International, 2011, 44(1):57-60.

[10] Ren L, Jiang T, Jia Z G, *et al.* Pipeline corrosion and leakage monitoring based on the distributed optical fiber sensing technology[J]. Measurement, 2018, 122:57-65.

[11] Mostafapour A, Davoudi S. Analysis of leakage in high pressure pipe using acoustic emission method[J]. Applied Acoustics, 2013, 74(3):335-342.

[12] Kaewwaewnoi W, Prateepasen A, Kaewtrakulpong P. Investigation of the relationship between internal fluid leakage through a valve and the acoustic emission generated from the leakage [J]. Measurement, 2010, 43(2):274-282.

[13] Martini A, Troncossi M, Rivola A. Leak Detection in Water-Filled Small-Diameter Polyethylene Pipes by Means of Acoustic Emission Measurements[J]. Applied Sciences, 2016, 7(1):2-15.

[14] Droubi M G, Reuben R L, Steel J I. Flow noise identification using acoustic emission (AE) energy decomposition for sand monitoring in flow pipeline[J]. Applied Acoustics, 2017, 113:5-15.

[15] Cui X, Yan Y, Guo M, *et al.* Localization of CO_2 Leakage from a Circular Hole on a Flat-Surface Structure Using a Circular Acoustic Emission Sensor Array[J]. Sensors, 2016, 16(11):1951-1965.

[16] Yu L, Li S Z. Acoustic emission (AE) based small leak detection of galvanized steel pipe due to loosening of screw thread connection[J]. Applied Acoustics, 2017, 120:85-89.

[17] Mostafapour A, Davoodi S. Leakage locating in underground high pressure gas pipe by acoustic emission method[J]. Journal of Nondestructive Evaluation, 2013, 32(2):113-123.

[18] Davoodi S, Mostafapour A. Gas leak locating in steel pipe using wavelet transform and cross-correlation method[J]. The International Journal of Advanced Manufacturing Technology, 2014, 70(5-8):1125-1135.

[19] Zhu S B, Li Z L, Zhang S M, *et al.* Natural gas pipeline valve leakage rate estimation via factor and cluster analysis of acoustic emissions[J]. Measurement, 2018, 125:48-55.

[20] Cui X, Yan Y, Ma Y, *et al.* Localization of CO_2, leakage from transportation pipelines through low frequency acoustic emission detection[J]. Sensors and Actuators A: Physical, 2016, 237(3):107-118.

[21] Yan Y, Cui X, Guo M, et al. Localization of a continuous CO_2 leak from an isotropic flat-surface structure using acoustic emission detection and near-field beamforming techniques[J]. Measurement Science and Technology, 2016,27(11):115105

[22] Wang T, Wang D, Pei Y, *et al.* Gas leak localization and detection method based on a multi-point ultrasonic sensor array with TDOA algorithm[J]. Measurement Science and Technology, 2015, 26(9): 095002.

[23] Liao P, Cai M, Shi Y, *et al.* Compressed air leak detection based on time delay estimation using a portable multi-sensor ultrasonic detector[J]. Measurement Science and Technology, 2013, 24(5): 055102.

[24] Abdulla M B, Herzallah R O, Hammad M A. Pipeline leak detection using artificial neural network: Experimental study[C]. International Conference on Modelling, 2013,328-332.

[25] Santos R B, Sousa E O D, Silva F V D, et al. Detection and on-line prediction of leak magnitude in a gas pipeline using an acoustic method and neural network data processing[J]. Brazilian Journal of Chemical Engineering, 2014, 31(1):145-153.

[26] Ribeiro A M, Grossi C D, Santos B F, *et al.* Leak Detection Modeling of a Pipeline Using Echo State Neural Networks[J]. Computer Aided Chemical Engineering, 2018, 43: 1231-1236.

[27] Zadkarami M, Shahbazian M, Salahshoor K. Pipeline leakage detection and isolation: An integrated approach of statistical and wavelet feature extraction with multi-layer perceptron neural network (MLPNN)[J]. Journal of Loss Prevention in the Process Industries, 2016, 43:479-487.

[28] Qu Z, Feng H, Zeng Z, *et al.* A svm-based pipeline leakage detection and pre-warning system[J]. Measurement, 2010, 43(4):513-519.

[29] Hou Q, Ren L, Jiao W, *et al.* An Improved Negative Pressure Wave Method for Natural Gas Pipeline Leak Location Using FBG Based Strain Sensor and Wavelet Transform[J]. Mathematical Problems in Engineering, 2013, 2013:1-8.

[30] Han Y, Tang B, Deng L. Multi-level wavelet packet fusion in dynamic ensemble convolutional neural network for fault diagnosis[J]. Measurement, 2018, 127:246-255.

[31] Rostek K, Morytko Ł, Jankowska A. Early detection and prediction of leaks in fluidized-bed boilers using artificial neural networks[J]. Energy, 2015, 89:914-923.